Received: 17 October 2023 | Revised: 29 January 2024 | Accepted: 23 February 2024 | Published online: 29 February 2024

RESEARCH ARTICLE

Journal of Optics and Photonics Research
2024, Vol. 00(00) 1–6
DOI: 10.47852/bonviewJOPR42021899

BON VIEW PUBLISHING

A Compact THz Photometer for Solar Flare Burst Studies from Space

M. A. Sumesh[1,*], S. P. Karanth[1] and K. V. Sriram[1]

[1]*Laboratory for Electro-Optics Systems, Indian Space Research Organization, India*

Abstract: Recent solar flare observations reveal the presence of THz components having a few orders of magnitude higher amplitude than the radio frequency and microwave radiations in the solar flare spectrum. This feature makes it remarkably beneficial for the detection of solar flares of low magnitudes such as Geostationary Operational Environmental Satellite (GOES) Class C, and M flares. Hence, space agencies including National Aeronautics and Space Administration (NASA) and European Space Agency (ESA) are gearing up with THz instruments for solar flare observations. In line with this, Laboratory for Electro-Optics Systems has completed the development of a photometer that operates in continuum THz band, from 1.5 to 15 THz. The entire electro-opto-mechanical design was carried out to realize a compact, light-weight, and power-efficient photometer to meet the size, mass, and power constraints posed by inherent resource limitations of experimental satellite platforms such as Nanosatellite, Microsatellite, and Polar Satellite Launch Vehicle's 4th Stage Orbital Platform (PS4-OP). A Cassegrain optical configuration was designed to collect the sun radiation with an aperture effective area of 0.0027 m^2 with ceramic low-pass filters and resonant mesh filter for selective perception of THz radiation, rejecting the huge background of visible and near infrared with a spectral selectivity of 10^7:1. Sensitivity of the photometer was estimated to be 41.5 K/mV in 1.5–15 THz band by calibration using a blackbody radiation source. The radiometric resolution of the payload is 125 solar flux unit (SFU) (1 SFU = 1 × 10^{-22} Wm^{-2}Hz^{-1}). The payload was successfully developed and space-qualified for its deployment in Nanosatellite or PS4-OP platform.

Keywords: THz, photometer, solar flare, solar flux unit

1. Introduction

Solar flares are violent eruptions of radiation caused by the sudden release of magnetic energy linked to sunspots. It is commonly understood that the effects of a solar flare are always detrimental to mankind. Increased X-ray and extreme ultraviolet (UV) emission during the solar flare events leads to modification of the electron density profile in the lower ionosphere due to enhanced ionization [1, 2]. These effects called sudden ionospheric disturbances [3] stimulate global positioning system malfunction [4] and disturbance in radio and wireless communication services [5, 6]. The stream of protons ejected from some of the very energetic flares can cause severe damage to unshielded satellites since these high energy protons are highly penetrating.

Solar hyperactivity results in solar proton events [7, 8], which raise the risk of computational and memory errors in on-board processors, failure of space instruments, and health risks for astronauts [9, 10]. The Earth's magnetic field is also impacted by solar disturbances, which can result in geomagnetic storms, which are brief interferences of the magnetosphere brought on by space weather disturbances linked to solar flares, coronal holes, or coronal mass ejections. Geomagnetic storms can cause disruptions in the power grid lines [11] and increased corrosion rate in the oil and gas pipelines [12]. Given that geomagnetic storms follow solar flares by 2–3 days [13, 14], the best course of action is to carry out continuous monitoring of solar flares in order to provide an early warning system that could protect not only infrastructure and resources but also precious lives.

Recently, a new component in THz was discovered in the solar flare spectrum, having higher peak amplitudes typically, few orders of magnitude higher than the microwave and radio frequency (RF) emission [15]. In addition to the RF and microwave radiations of the solar flare spectrum where the flux shows a positive slope at lower frequencies and a negative slope at higher frequencies, certain bursts have a separate spectral feature in the sub-THz regime wherein the flux increases with frequency. These radiations are attributed to be incoherent synchrotron radiation emitted by the high energy electron beams accelerated in the magnetic fields associated with solar flare. Another model suggests free-free emissions from the high temperature (10^4–10^6 K) plasma of solar flux ribbons [16]. However, no firm conclusion on the real origin of the THz is arrived yet and systematic observations are required to unravel the mystery of origin of THz and sub-THz radiation in solar flares.

The THz components in the solar flare spectrum have a few orders of magnitude higher amplitude than the RF and microwave radiations [15] which makes it beneficial for the detection of solar flares of low magnitudes such as C, and M flares of Geostationary Operational Environmental Satellite (GOES) Class. Ground-based observatories are envisaged for solar flare observation in 0.2, 0.4, 0.84, 1.4, and 30 THz [15, 17–19]. Subsequently, THz photometers in 3 and 7 THz ranges were developed for solar burst observation from stratospheric

*Corresponding author: M. A. Sumesh, Laboratory for Electro-Optics Systems, Indian Space Research Organization, India. Email: sumesh@leos.gov.in

balloon platforms [20]. However, no reports are available on observation of solar flare in the continuum THz band.

In Laboratory for Electro-Optics Systems (LEOS), Detector Development Division has been involved in the development of broad band THz detectors since 2015 under a technology development project [21, 22]. Further to the successful development of THz detector technology in-house, the development of a photometer for solar flare transient burst observation is taken up in line with the progress made by other space agencies as mentioned above.

This paper presents the development and space qualification of a THz photometer for observing solar flare bursts from a spaceborne platform in the continuum band (1.5–15 THz).

2. Design of THz Photometer

The spacecraft interface and payload's optical, mechanical, and electrical configurations have been designed to meet the limitations of the Nanosatellite platform, including:

1) weight less than 5 kg
2) center of gravity within 50 mm from the payload mounting interface
3) maximum power consumption 8 W.

The primary challenge is suppressing the solar emission in visible and infrared regions without much attenuation to the THz radiation, which is found to be a very weak signal (0.67 mWm^{-2} at 3 THz, whereas the total solar irradiance is 1378 Wm^{-2}). Planck's radiation law is used for estimation of the solar irradiation in outer space. The majority of the solar emission (99.5%) falls in the shorter wavelength region (<5 μm) with a peak at ~500 nm. Planck's radiation law [23, 24] was used for estimating the spectral radiant emittance of the blackbody in $Wm^{-2}sr^{-1}THz^{-1}$.

$$L(f,T) = \frac{2hf^3}{c^2}\left(\frac{1}{e^{\left(\frac{hf}{k_B T}\right)} - 1}\right) \tag{1}$$

where

f = frequency,
h = Planck's constant
T = temperature
c = speed of light in vacuum
k_B = Boltzmann's constant

Radiant emittance $M(T)$ is the integral of $L(f,T)$ with respect to f for the given temperature of the Sun photosphere. Considering the transmission spectrum of the THz window, $\eta(f)$ the radiant emittance is obtained as:

$$M(T) = \int_{1.5}^{15} \eta(f)\frac{2hf^3}{c^2}\left(\frac{1}{e^{\left(\frac{hf}{k_B T}\right)} - 1}\right) df \tag{2}$$

The optical power received by the detector ϕ_{det} is further estimated as:

$$\phi_{det} = M(T) A_{bb} \Omega_{det,bb} \tag{3}$$

where A_{bb} = area of blackbody and $\Omega_{det,bb}$ = solid angle subtended by the detector. It is clear from Figure 1 that, as compared to the visible-infrared regime, the emission of radiation in the terahertz range is very low. This proportion turns out to be approximately 0.2 ppm in the case of 3 THz. The uncooled THz detector used in the photometer is sensitive to the broad spectrum of solar radiation, right from visible, infrared, and terahertz, and it makes the measurement quite challenging in the presence of the background solar radiation.

Figure 1
Solar spectral emission at airmass zero (AM0) condition

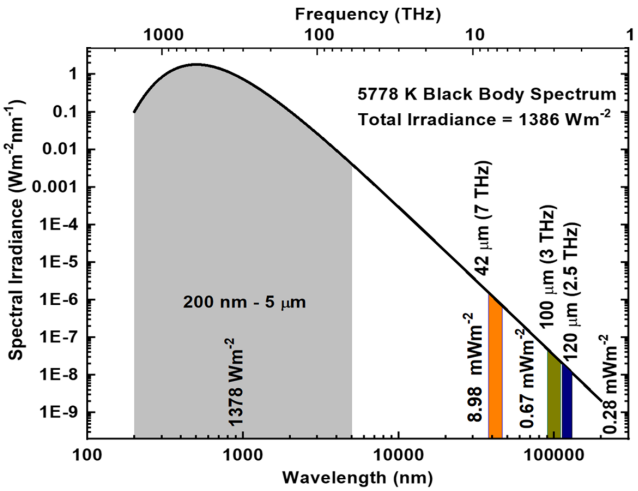

To accurately measure the THz radiation emitted by the Sun, specialized filtering techniques with spectral selectivity as high as 10^7 are needed to suppress the visible and infrared regions, while detecting the THz radiation in the designated band of frequency. This is particularly true for thermal detectors, whose spectral response spans a large range from UV to THz.

A cascade of technologies was used to achieve high spectral selectivity. It includes micro-roughening of reflective optical components and the adoption of resonant mesh filter [25] for selection of THz radiation band. With this combination, the transmittance of UV, visible, and near-infrared radiations is suppressed to < 1% for wavelengths up to 5 μm as shown in Figure 2. Further band rejection is achieved by the usage of ceramic low-pass filter with cut-in at

Figure 2
The reflectance of the roughened metal mirror and the transmittance characteristics of the resonant metal mesh THz filter

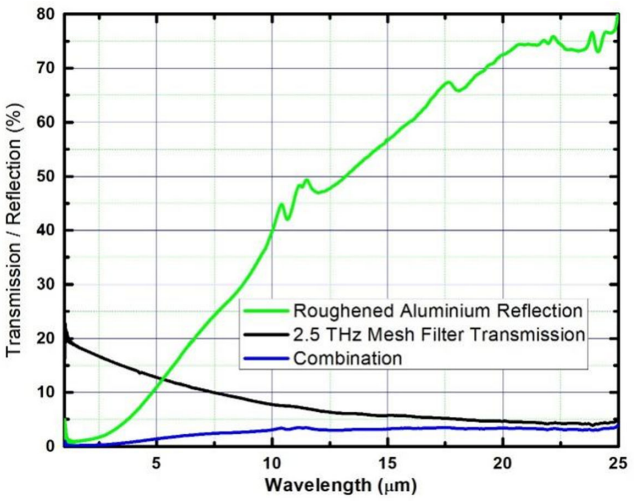

21 μm (off-band transmission 0.1%) and germanium window for further blocking the short wavelength radiations.

Because of its compact size and ease of integration with the detector system, the front-end optics is designed with a reflective optical system based on the Cassegrain configuration. To achieve an IFOV of ± 1° with detector size of 2 mm × 2 mm, an optical design consisting of a primary concave mirror measuring 75 mm in diameter and a secondary convex mirror measuring 20 mm in diameter was implemented leading to 100 mm effective focal length. Aluminum alloy, AA6061-T6, was used for fabricating the mirrors, and the assembly consisting of the telescope, detector, and the THz filters was then evaluated for optical performance, field of view, and focal length.

Modulation of the optical radiation is achieved by integrating a resonant fork optical chopper (CH-10 from Electro Optical Products Corporation (EOPC), USA). This resonant fork modulator ensures jitter-free operation while tuned at 20 Hz with high stability (better than 0.005%), matched to the optimum operating frequency of the detector.

Compared to the continuum spectrum, solar emission at the THz spectrum is extremely low, making it very difficult to design front-end electronics for signal processing to meet the dynamic range requirement. Such deeply buried signals can be extracted from noisy ambient environments only by lock-in amplifier-based electronics [26]. A dynamic range of up to 110 dB was reached by designing and integrating a very small lock-in-amplifier with sensor electronics. The output of the front-end signal conditioner is an analog voltage, proportional to an incident THz radiation. This voltage is converted to digital by a 16 bit sigma-delta analog to digital converter (ADC) at 128 Hz rate so that the on-board microcontroller (Atmega328P) could process it further. Figure 3 shows the instrument architecture block diagram.

Figure 3
Internal architecture of the photometer

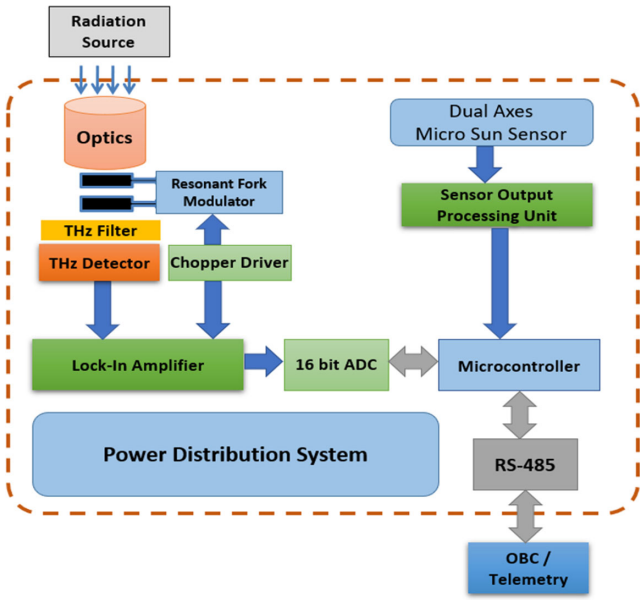

The payload uses a serial peripheral interface (SPI) for communication with the on-board computer of the Nanosatellite. Additionally, for interface with other platforms such as PS4-OP [27], a serial communication protocol based on the RS485 interface was also implemented. In order to perform autonomous measurement of the sun pointing angle, a Dual Axes Micro Sun Sensor was deployed on the front face of the photometer. The Micro Sun Sensor provides the exact angle between the optical axis of the THz photometer and the sun rays. This feature enables cosine correction to compensate for the output variation with sun angle within the FOV.

The electronics circuit consists of lock-in-amplifier, microcontroller, 16-bit ADC, sensor output processing unit, power distribution system, and digital interface circuit where accommodated in a single printed circuit board while the chopper driver was made as a separate one.

Multiple factors were considered while designing the instrument to keep it light weight and low power. Cassegrain telescope was chosen due to its inherently compact design. The telescope mirrors (both primary and secondary) were made of aluminum. The telescope barrel and the spider for secondary mirror, and the mechanical housings were light-weighted by design and fabricated using precipitation hardened aluminum alloy Al6061-T6. Instead of a conventional mechanical chopper, a resonant fork optical modulator was chosen that significantly reduced the weight of the system. All these efforts could finally keep the weight of the entire payload within 1.5 kg.

Payload configuration was designed to keep the heavier components and systems of the instrument at lower region in order to have the center of gravity close to the base. The electronic cards, DC-DC convertor, and harness were contained in the mechanical housing that forms the base of the payload, while the light-weighted telescope which is, by and large a hollow structure, was mounted on top as shown in Figure 4 and this approach resulted in maintaining the center of gravity of the payload within 50 mm from the base as required by Nanosatellite platform.

Figure 4
THz photometer payload realized

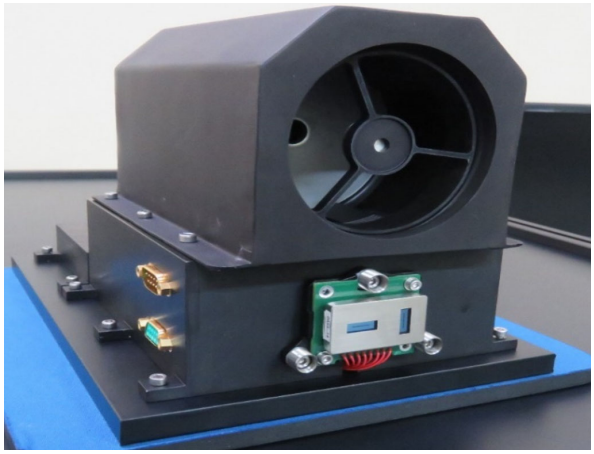

Adoption of commercial off-the-shelf components provides the designer with freedom to choose electronic devices of tiny foot print, low power, and high performance. Usage of a microcontroller instead of the traditional space-grade field programmable gate array (FPGA) has significantly reduced the circuit complexity and power consumption. Usage of a resonant fork optical modulator significantly reduced the power consumption as compared to conventional optical choppers based on brushless DC/synchronous motors. With all these efforts, the power consumption of the payload was limited to 4.5 W.

3. Photometer Characterization

The cumulative noise of the instrument, which comprises of contributions from electronics, mechanical (vibrations from resonant fork optical modulator), and detector noise, was measured over a period of time and follows to the Gaussian nature with a standard deviation of 30 μV_{rms}. Figure 5 shows the temporal fluctuations in the output of the THz photometer while tested with a 1073 K National Institute of Standards and Technology calibrated blackbody (Model SR-20, Make CI systems, Israel).

Figure 5
The output of the THz photometer when tested with 1073 K blackbody

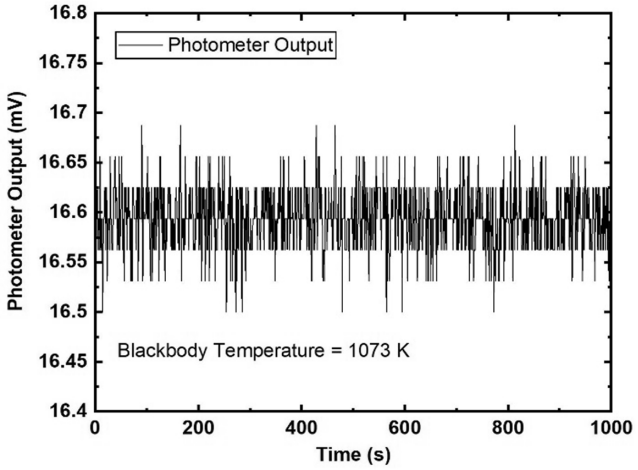

Further, to evaluate the sensitivity of the photometer to temporal variations in solar flux, laboratory tests have been carried out using a blackbody radiation source with an off-axis parabolic collimator (divergence ± 0.25°) as an artificial sun. The THz photometer was calibrated against blackbody at various temperatures and 41.5 K/mV sensitivity was observed as shown in Figure 6.

Figure 6
Calibration of THz photometer using blackbody radiation source

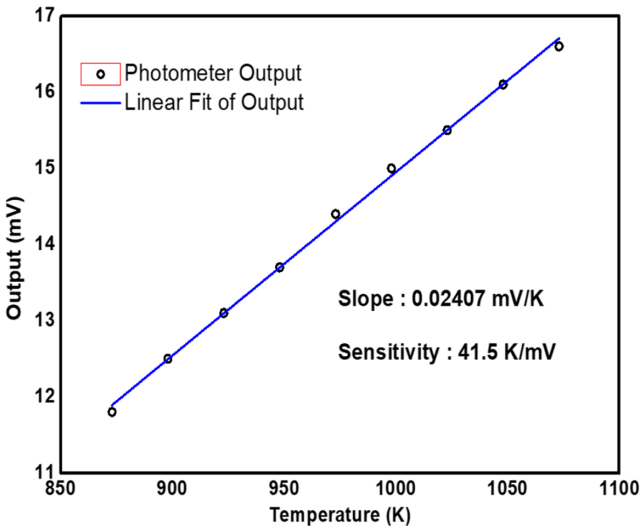

The radiometric resolution of a photometer is given by:

$$\Delta S = \frac{2k_B \Delta T}{A_e} \tag{4}$$

where A_e is the effective area of the telescope aperture and k_B is the Boltzmann's constant. ΔT is the minimum resolvable excess temperature transient, which in turn is obtained as the product of photometer noise and sensitivity and is 1.24 K for the present case. The effective area of the telescope aperture is given by:

$$A_e = \eta_{Transmission} \times A_{PrimaryOptics} \tag{5}$$

where $\eta_{Transmission}$ is the optical transmittance and $A_{PrimaryOptics}$ is the physical area of the primary mirror. The primary mirror area is 0.0044 m^2, and the transmittance is 60% considering the efficiency of all the optical components. The effective area, A_e, is 0.0027 m^2. The radiometric resolution of the instrument in terms of solar flux unit (SFU) is 125 SFU (1 SFU = 1×10^{-22} $Wm^{-2}Hz^{-1}$).

Table 1 lists the technical specifications of the photometer.

Table 1
Specifications of the THz photometer

Sl. No.	Specification	Value
1	Operating frequency	Continuum (1.5–15 THz)
2	Resolution	125 SFU
3	Field of view	± 1°
4	Optics configuration	Cassegrain
5	Detector type	$LiTaO_3$ based uncooled pyroelectric THz detector
6	Detector frequency range	0.1–30 THz
7	Weight	1.5 kg
8	Size (mm^3)	140 × 142 × 156
9	Power requirement	9–18 V DC
10	Power consumption	4.5 W
11	Communication	SPI/RS485
12	Data update rate	Up to 10 samples/second
13	Location	+Ve yaw panel
14	Orientation	–Ve pitch (Sun pointing)

4. Space Qualification of the Package

It is proposed to fly the THz photometer instrument in a suitable space platform such as a Nanosatellite, PS4-OP, or Microsatellite. The objective of the first flight is to calibrate the instrument in the continuum THz band (1.5–15 THz spectral range) from outer space and to study the solar flare burst during the mission period. PS4-OP and Nanosatellites provide excellent platforms for carrying out demonstration of new technologies while providing experimental support for innovative technology development before it can be flown in a more serious mission. Test Plan Committee of Polar Satellite Launch Vehicle (PSLV) project has formulated a detailed qualification plan for the payloads to be flown as part of the PS4-OP. Test conditions as applicable to Proto FM (single flight model) were adopted for qualifying the THz photometer. Details of the environmental tests are provided in Figure 7.

Qualification of the photometer was completed as per the environmental test levels for PSLV components and subassemblies suggested by Test Plan Committee of PSLV project. Payload performance was satisfactory throughout the qualification program and passed all the tests. The root mean square noise and signal to

Figure 7
Test matrix adopted for qualification of THz photometer

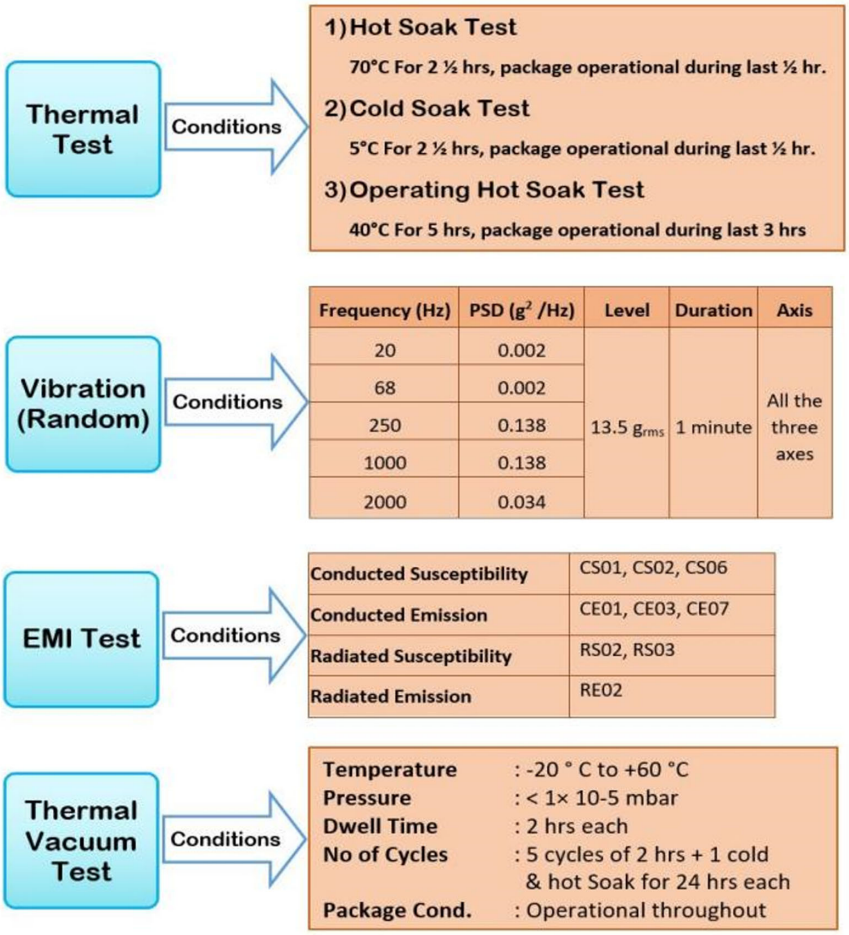

noise ratio remained unchanged during all levels of space qualification exercise.

5. Conclusion

A THz photometer was designed and developed for observation of solar flare in continuum THz band of 1.5–15 THz at LEOS and is qualified for space deployment. The instrument is capable of detecting solar flares of intensity as low as 125 SFU, which corresponds to GOES Class C and higher magnitude. Currently, developed THz photometer, by studying the solar flare in continuum THz band from a satellite platform, will unravel new insights into complex and still mysterious emission phenomena during solar hyperactivities. Further, due to the higher magnitude of the THz signals as compared to the RF and microwave counterparts, deployment of the instrument for solar flare detection can generate early warning signals on the potential threats posed by solar storms well in advance (3–5 days) for safeguarding space infrastructure as well as astronauts. It is planned to deploy the payload in an experimental space platform such as Nanosatellite, PS4-OP, or Microsatellite for calibration against quiescent sun background and to detect any flare-induced THz signatures during the mission span in comparison with the GOES flare classifications.

Acknowledgement

The development team would like to acknowledge Shri. M. Sankaran, Director URSC (Chairman, Apex Committee for PS4-OP) for his support and guidance during the development and in reviewing its adequacy for detecting solar flare by on-board observations.

Ethical Statement

This study does not contain any studies with human or animal subjects performed by any of the authors.

Conflicts of Interest

The authors declare that they have no conflicts of interest to this work.

Data Availability Statement

Data are available from the corresponding author upon reasonable request.

Author Contribution Statement

M. A. Sumesh: Conceptualization, Methodology, Software, Validation, Formal analysis, Investigation, Data curation, Writing – original draft, Writing – review & editing, Visualization, Supervision, Project administration. **S. P. Karanth:** Conceptualization, Methodology, Formal analysis, Investigation, Resources, Writing – review & editing, Visualization, Supervision, Project administration. **K. V. Sriram:** Validation, Visualization, Supervision, Project administration.

References

[1] Briand, C., Clilverd, M. A., Inturi, S., & Cecconi, B. (2022). Role of hard X-ray emission in ionospheric D-layer disturbances during solar flares. *Earth, Planets and Space*, *74*(1), 41. https://doi.org/10.1186/s40623-022-01598-2

[2] Donnelly, R. F. (1968). The X-ray and extreme ultraviolet radiation of the August 28, 1966 proton flare as deduced from sudden ionospheric disturbance data. *Solar Physics*, *5*(1), 123–126. https://doi.org/10.1007/bf00147126

[3] Dellinger, J. H. (1937). Sudden disturbances of the ionosphere. *Proceedings of the Institute of Radio Engineers*, *25*(10), 1253–1290. https://doi.org/10.1109/jrproc.1937.228657

[4] Filić, M., & Filjar, R. (2019). On correlation between SID monitor and GPS-derived TEC observations during a massive ionospheric storm development. In *URSI Asia-Pacific Radio Science Conference*, 1–4. https://doi.org/10.23919/URSIAP-RASC.2019.8738664

[5] Lanzerotti, L. J. (2007). Space weather effects on communications. In V. Bothmaer & I. A. Daglis (Eds.), *Space weather: Physics and effects* (pp. 247–268). Springer. https://doi.org/10.1007/978-3-540-34578-7_9

[6] Omatola, K. M., & Okeme, I. C. (2012). Impacts of solar storms on energy and communications technologies. *Archives of Applied Science Research*, *4*(4), 1825–1832.

[7] Shea, M. A., & Smart, D. F. (1990). A summary of major solar proton events. *Solar Physics*, *127*(2), 297–320. https://doi.org/10.1007/bf00152170

[8] Smart, D. F., & Shea, M. A. (1989). Solar proton events during the past three solar cycles. *Journal of Spacecraft and Rockets*, *26*(6), 403–415. https://doi.org/10.2514/3.26086

[9] Bentoutou, Y., & Bensikaddour, E. H. (2015). Analysis of radiation induced effects in high-density commercial memories on-board Alsat-1: The impact of extreme solar particle events. *Advances in Space Research*, *55*(12), 2820–2832. https://doi.org/10.1016/j.asr.2015.02.032

[10] Croley, D. R., Garrett, H., Murphy, G. B., & Garrard, T. L. (1995). Solar particle induced upsets in the TDRS-1 attitude control system RAM during the October 1989 solar particle events. *IEEE Transactions on Nuclear Science*, *42*(5), 1489–1496. https://doi.org/10.1109/23.467946

[11] Stauning, P. (2002). High-voltage power grid disturbances during geomagnetic storms. In *Proceedings of the Second Solar Cycle and Space Weather Euroconference*, *477*, 521–524.

[12] Gummow, R. A., & Eng, P. (2002). GIC effects on pipeline corrosion and corrosion control systems. *Journal of Atmospheric and Solar-Terrestrial Physics*, *64*(16), 1755–1764. https://doi.org/10.1016/s1364-6826(02)00125-6

[13] Park, Y. D., Moon, Y. J., Kim, I. S., & Yun, H. S. (2002). Delay times between geoeffective solar disturbances and geomagnetic indices. *Astrophysics and Space Science*, *279*, 343–354. https://doi.org/10.1023/A:1015158005020

[14] Yermolaev, Y. I., Yermolaev, M. Y., Zastenker, G. N., Zelenyi, L. M., Petrukovich, A. A., & Sauvaud, J. A. (2005). Statistical studies of geomagnetic storm dependencies on solar and interplanetary events: A review. *Planetary and Space Science*, *53*(1–3), 189–196. https://doi.org/10.1016/j.pss.2004.09.044

[15] Kaufmann, P., White, S. M., Marcon, R., Kudaka, A. S., Cabezas, D. P., Cassiano, M. M., . . . , & de Souza, R. V. (2015). Bright 30 THz impulsive solar bursts. *Journal of Geophysical Research: Space Physics*, *120*(6), 4155–4163. https://doi.org/10.1002/2015ja021313

[16] Kontar, E. P., Motorina, G. G., Jeffrey, N. L. S., Tsap, Y. T., Fleishman, G. D., & Stepanov, A. V. (2018). Frequency rising sub-THz emission from solar flare ribbons. *Astronomy & Astrophysics*, *620*, A95. https://doi.org/10.1051/0004-6361/201834124

[17] de Castro, C. G. G., Raulin, J. P., Valio, A., Alaia, G., Alvarenga, V., Bortolucci, E. C., . . . , & Zaquela, M. (2020). HATS: A ground-based telescope to explore the THz domain. *Solar Physics*, *295*(4), 56. https://doi.org/10.1007/s11207-020-01621-3

[18] Lindsey, C., Kopp, G., Becklin, E. E., Roellig, T., Werner, M. W., Jefferies, J. T., . . . , & Mickey, D. L. (1990). Far-infrared intensity variations caused by 5 minute oscillations. *The Astrophysical Journal*, *350*, 475–479. https://doi.org/10.1086/168401

[19] Lindsey, C., & Kopp, G. (1995). Submillimeter radiometry of sunspots. *The Astrophysical Journal*, *453*, 517–521. https://doi.org/10.1086/176413

[20] Kaufmann, P., Abrantes, A., Bortolucci, E. C., Correia, E., Diniz, J. A., Fernandez, G., . . . , & Zakia, M. (2012). SOLAR-T: Terahertz photometers to observe solar flare emission on stratospheric balloon flights. In *Proceedings of SPIE: Space Telescopes and Instrumentation 2012: Optical, Infrared, and Millimeter Wave*, *8442*, 84424L. https://doi.org/10.1117/12.926072

[21] Sumesh, M. A., Karanth, S. P., Thomas, B., Rao, G. M., Viswanathan, M. R., Chakraborty, P., & Rao, G. N. (2017). Performance-enhanced bolometric terahertz detectors based on V_2O_5 for 15 to 30 THz. *Journal of Infrared, Millimeter, and Terahertz Waves*, *38*(2), 135–142. https://doi.org/10.1007/s10762-016-0326-1

[22] Sumesh, M. A., Thomas, B., Vijesh, T. V., Mohan Rao, G., Viswanathan, M. R., & Karanth, S. P. (2018). Optically immersed bolometer IR detectors based on V_2O_5 thin films with polyimide thermal impedance control layer for space applications. *Journal of Infrared, Millimeter, and Terahertz Waves*, *39*(1), 6–23. https://doi.org/10.1007/s10762-017-0446-2

[23] Marr, J. M., & Wilkin F. (2012). A better presentation of Planck's radiation law. *American Journal of Physics*, *80*(5), 399–405. https://doi.org/10.1119/1.3696974

[24] Lewis, R. A. (2013). *Terahertz physics*. UK: Cambridge University Press. https://doi.org/10.1017/cbo9781139088190

[25] Porterfield, D. W., Hesler, J. L., Densing, R., Mueller, E. R., Crowe, T. W., & Weikle, R. M. (1994). Resonant metal-mesh bandpass filters for the far infrared. *Applied Optics*, *33*(25), 6046–6052. https://doi.org/10.1364/AO.33.006046

[26] Liu, Y. L., & Zhang, R. (2012). AD630 lock-in amplifier circuit for weak signal. *Advanced Materials Research*, *482–484*, 975–980. https://doi.org/10.4028/www.scientific.net/amr.482-484.975

[27] Sanood, U., Sandeep, M., Bapista, A., Suresh Nair, C. G., Lal, M. J., & Biju, S. R. (2023). PS4-orbital platform: An ideal suite for scientific experiments. In *Advances in Small Satellite Technologies: Proceedings of National Conference on Small Satellite Technology and Applications*, 77–85. https://doi.org/10.1007/978-981-19-7474-8_7

How to Cite: Sumesh, M. A., Karanth, S. P., & Sriram, K. V. (2024). A Compact THz Photometer for Solar Flare Burst Studies from Space. *Journal of Optics and Photonics Research*. https://doi.org/10.47852/bonviewJOPR42021899